AIAA JOURNAL
Vol. 49, No. 7, July 2011

Numerical Analysis of an Oscillating-Wing Wind and Hydropower Generator

M. A. Ashraf,* J. Young,† and J. C. S. Lai‡
University of New South Wales at the Australian Defense Force Academy, Canberra, Australian Capital Territory 2600, Australia
and
M. F. Platzer§
AeroHydro Research and Technology Associates, Pebble Beach, California 93953

DOI: 10.2514/1.J050577

The extraction of energy from wind or water streams is generally accomplished by means of rotary systems. However, it is recognized and it has been demonstrated that oscillating wings can also be used for this purpose. A newly developed oscillating-wing wind and hydropower generator is described. Its potential for the generation of electric power from tidal flows and high-altitude jet streams is studied using two-dimensional Navier–Stokes simulations at $Re = 20,000$. Results for a single NACA 0014 wing power generator undergoing nonsinusoidal pitch–plunge motion indicate around 17% increase in power generated and around 15% increase in efficiency over that for sinusoidal motion. Two airfoils operating in tandem, undergoing both sinusoidal and nonsinusoidal motions, are also studied. It is found that for sinusoidal motion both averaged power output and efficiency per foil are reduced by around 20% for tandem configurations compared with a single foil in sinusoidal motion, and similar performance reductions are experienced for nonsinusoidal motions.

Nomenclature

a	=	plunge amplitude, m
C_P	=	instantaneous power coefficient, $P/0.5\rho U_\infty^3 c$
$C_{P\text{mean}}$	=	time-averaged power coefficient, $\bar{P}/0.5\rho U_\infty^3 c$
C_p	=	surface pressure coefficient
c	=	chord, m
d	=	maximum total transverse distance swept by any portion of the foil chord line
f	=	flapping frequency, Hz
h	=	nondimensional plunge amplitude, a/c
k	=	reduced frequency, $2\pi fc/U_\infty$
L	=	transverse force on the foil, N
M	=	moment about the foil pivot point, Nm
P	=	power developed, $LV_y + M\theta$
$\bar{P}$	=	time-averaged power
P_a	=	maximum power available, $0.5\rho U_\infty^3 d$
Re	=	Reynolds number based on chord
T	=	period of oscillation
t	=	time
U_∞	=	freestream velocity, m/s
V_y	=	translational velocity, m/s
X_{shift}	=	distance between tandem foil pivot points, nondimensionalized by chord
ΔT_R	=	stroke reversal time, as a fraction of the flapping period
η	=	efficiency of power extraction, $\bar{P}/P_a$
$\dot{\theta}$	=	pitch motion velocity, rad/s
θ_o	=	pitch motion amplitude, rad
ϕ	=	phase angle between pitch and plunge motions of a single foil, rad (+ve indicates pitch leads plunge)
ψ	=	phase angle between motions of tandem foils, rad (+ve indicates trailing foil leads)
ω	=	circular oscillation frequency, rad/s

Presented as Paper 2009-1211 at the 47th AIAA Aerospace Sciences Meeting Including the New Horizons Forum and Aerospace Exposition, Orlando, FL, 5–9 January 2009; received 26 March 2010; revision received 7 January 2011; accepted for publication 11 February 2011.

*Research Associate, School of Engineering and Information Technology (Corresponding Author).
†Senior Lecturer, School of Engineering and Information Technology. Member AIAA.
‡Professor, School of Engineering and Information Technology. Associate Fellow AIAA.
§Senior Partner. Fellow AIAA.

I. Introduction

IN RECENT times, the increase in global power generation needs has raised two major issues, namely decreasing availability of fossil fuels for power generation and their impact on the global climate. These two issues are the main driving force behind the search for alternative methods to produce energy from renewable sources. Among several renewable sources, power extraction from wind or water streams is an attractive alternative method. This extraction is generally accomplished by means of rotary systems. However, it is recognized and it has been demonstrated that oscillating wings (simultaneously pitching and plunging) can also be used for this purpose [1].

The extraction of power from an airstream is a phenomenon well known to aeronautical engineers. Consider an airfoil that is free to oscillate vertically and in pitch, as shown in Fig. 1. If the combined oscillation occurs in such a manner that there is a 90 deg phase angle ϕ between the pitch and the plunge (vertical) motion, then the aerodynamic lift is always in the same direction as the motion of the airfoil, as shown in Fig. 1a. In this case, work is done by the air on the airfoil throughout the complete cycle. In other words, the airfoil is extracting energy out of the air flow. On the other hand, if the phasing between pitch and plunge is zero, as shown in Fig. 1b, then during parts of the cycle the aerodynamic lift opposes the motion and no net work is done on the airfoil. The type of flutter shown in Fig. 1a can easily occur on airplane wings, for certain values of the bending and torsional stiffnesses of the wing. Clearly, this phenomenon can also be used for power generation.

It should be noted here that up until recently, interest in flapping foils has been focused on thrust generation [2–6]. As seen in Fig. 1, the angle of attack α during the flapping cycle determines the sign of aerodynamic forces generated by the flow and, hence, propulsion or thrust generation. The application of flapping foils as a propulsor or a

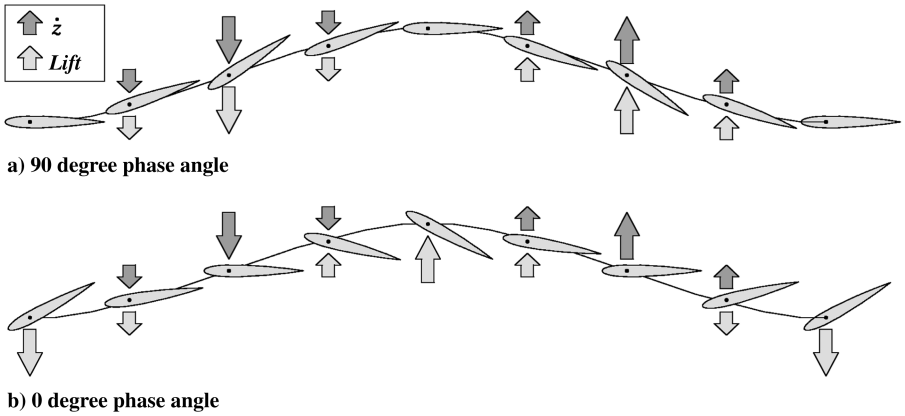

Fig. 1 Bending-torsion airfoil flutter.

power generator is determined by a feathering parameter, $\chi = \theta_o / \arctan(h\omega/U_\infty)$ [7,8]. Here, θ_o is the pitch amplitude, h is the nondimensional plunge amplitude, ω is the circular oscillation frequency, and U_∞ is the freestream velocity. The three main regimes of flow over flapping foils are propulsion regime ($\chi < 1$, and α remains positive when the foil passes through the mean position), power extraction regime ($\chi > 1$, and α remains negative when the foil passes through the mean position), and feathering regime (no net thrust or power extraction, $\chi = 1$, and $\alpha = 0$ when the airfoil passes through the mean position).

Whereas in the last decade there has been increasing and intense interest in the aerodynamics of flapping foils for propulsion of micro air vehicles [2–6], the use of flapping foils for power generation has largely remained unexplored. A large number of studies related to natural flyers or simple flapping airfoils/wings show that flapping wings at low Reynolds number are capable of generating large aerodynamic forces. This has been attributed largely to the leading-edge vortices (LEVs) that form due to leading-edge separation at low Reynolds number and higher angles of attack during a flapping cycle. It is envisaged that the desired flapping-wing power generators may also exploit this unsteady mechanism and achieve comparable or better performances than do the existing rotary blade/wing technologies.

In 1981, McKinney and Delaurier [1] performed analytical and experimental analyses of flow over a flapping-wing power generator in order to examine its feasibility. They used a fixed plunge amplitude, $h = 0.6$, while varying the phase between pitching and plunging motions, to conduct their experiments. These results showed the importance of unsteady aerodynamics and reported higher power and efficiency than did their linear analytical analysis. They reported power extraction efficiency as high as 28.3% at the maximum angle of attack of 30° and a phase difference between pitching and plunging of 110°. Though the results presented by McKinney and Delaurier were very encouraging, it is suspected that the full benefits of delayed stall and the associated LEV formation at high-pitch amplitudes were not fully exploited in their experiment, as they considered only moderate pitch and plunge amplitudes.

Further, a laboratory-scale hydropower generator was built and tested by Platzer and his associates [9–12]. The mechanical control system to set the phasing between the pitch and plunge motions is described by Davids [9]. The experience gained from this hydropower generator was applied in the design of a second power generator, which used two hydrofoils in a tandem arrangement [10]. The mechanical control system to set the phasing between the pitch and plunge motions of the two hydrofoils and between the motion of the two hydrofoils is described by Lindsey [10]. Two-dimensional panel code and Navier–Stokes (NS) computations were employed to estimate the performance [12]. A 90 deg phasing between the motion of the two hydrofoils made the generator self-starting, regardless of the initial hydrofoil positions. Also, because of this mutual reinforcement between the two hydrofoils, the flywheel used on the first generator was not required in this setup. The water tunnel tests of this second generator, in fact, show that the tandem arrangement results in a smoother running machine. The details of these tests can be found in Lindsey [10] and Jones et al. [12]. More recently, Platzer et al. [13] developed an oscillating-wing power generator that requires no elaborate mechanism to enforce the wing's pitch–plunge motion at the proper phase angle between the pitch and plunge motions. The basic principle of the new generator is shown in Fig. 2. An airfoil is shown that can slide on a rail guide. Furthermore, it can pitch about a pitch axis that is located downstream of the midchord point. This ensures that the airfoil is statically unstable, so that it deflects to an increasing pitch angle until it is stopped by a mechanical restraint. In Fig. 2, the flow is assumed to be from left to right, and the airfoil is, therefore, sliding to the left because of the lift generated by the airfoil's pitch angle. However, the airfoil starts to turn counterclockwise as soon as the airfoil's "finger" (extending from the leading edge, as seen in Fig. 2) starts to touch the control rod shown in Fig. 2. An aerodynamic moment is generated that initiates the stroke reversal by pitching the airfoil past the zero pitch angle. As a result, the airfoil is now generating a lift force in the opposite direction, and the airfoil starts to slide to the right. The process repeats itself at the other end, and a square-wave-type oscillation is being generated. Hence, the required phase angle between the pitch and plunge oscillations of the wing is produced by purely aerodynamic means. This simple yet effective mechanism provides the motivation for the analysis of nonsinusoidal motions considered in the current numerical investigation.

Recently, Kinsey and Dumas [7] employed a NS solver to conduct a parametric study of a sinusoidally plunging and pitching NACA 0015 airfoil at a Reynolds number of 1100, operating in a power extraction regime. The phase angle between the pitching and plunging motions was prescribed. They mapped the efficiency of the flapping airfoil generator as a function of the frequency and pitching amplitude, at a fixed plunge amplitude of $h = 1.0$ and a phase difference between pitching and plunging of 90°. They reported

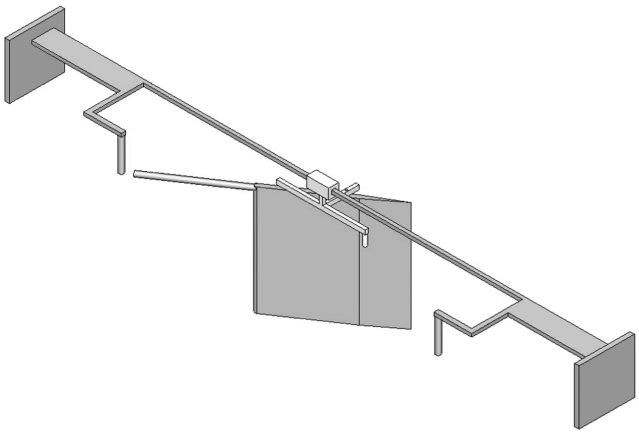

Fig. 2 Aerohydrodynamically controlled power generator (wing in midstroke).

power extraction efficiencies as high as 34%, at a pitch amplitude of $\theta_o \approx 76^\circ$ and a reduced frequency of $k \approx 0.88$. They found that dynamic stall plays an important role in maximizing the power and efficiency. They suggested that the timing of the formation and shedding of a LEV during a flapping cycle is very important for achieving higher efficiency in a flapping-wing power generator. Though Kinsey and Dumas performed a thorough numerical analysis of flapping airfoil power generators at extended range of pitch and plunge amplitudes, they did not investigate the effect of varying the phase difference between pitch and plunge motion for a sinusoidally pitching and plunging airfoil generator. Also, they only considered sinusoidal motions, and it is suspected that nonsinusoidal motions may increase the power output capacity of the proposed flapping-wing power generators, because Kaya and Tuncer [14] have shown that nonsinusoidal motions perform better for thrust generation than sinusoidal motions.

The experiments of Jones et al. [12] and Platzer et al. [13] suggest that the power generation capacity may be increased by using square-wave-type oscillations and airfoils oscillating in tandem arrangement. The motivation for the tandem configuration analysis also comes from the results reported by Akhtar et al. [15] and Lehmann [16]. Akhtar et al. [15] reported that for a tandem foil configuration with $X_{\text{shift}} = 1$ chord length of the trailing foil (distance between the trailing edge of the leading foil and the leading edge of the trailing foil) at $Re = 1200$, a phase difference of 48° between the motion of the two foils augments the thrust output by three times and the propulsive efficiency by two times over the trailing-foil-only configuration. Lehmann [16] studied force production by insect tandem wings (mechanical dragonfly model), to analyze power expenditure and aerodynamic efficiency. He reported that, in four-winged insects, wing phasing determines both mean force production and power expenditures for flight. Maximum combined fore–hind wing lift is produced for a phase difference of a quarter of a cycle between hind and fore wings, with one chord-length separation. By increasing the distance between the two tandem wings, lift and drag approach the performance of a single wing operating in isolation, due to increasing loss of vorticity in the wake.

The objective of this study, therefore, is to explore numerically the effect of phase difference between prescribed pitch and plunge sinusoidal motion and the effect of prescribed nonsinusoidal foil motion on power generation for both single and tandem foil configurations. NS simulations are used to explore the influence of phase between pitch and plunge motion on the power output of a single airfoil power generator undergoing sinusoidal motion. Then, a single airfoil power generator undergoing nonsinusoidal motion is considered, and the effect of various parameters (such as oscillation frequency, plunge amplitude, pitch amplitude, and phase between pitch and plunge) on the power extracted and on efficiency is assessed. Lastly, two airfoils in tandem configuration are considered, undergoing sinusoidal and nonsinusoidal motions. The effect of varying the distance between the two airfoils and the phase difference between the motions of the two foils on the power output of tandem power generators has been examined. Unless otherwise indicated, all calculations were performed for laminar flows at $Re = 20,000$. This Reynolds number is chosen for two reasons: for the availability of experimental data on plunging airfoils for validation and for the benefits associated with low-Reynolds-number flapping-wing aerodynamics, i.e., formation of LEVs causing augmented lift force, which would help achieve higher power output. A first version of this paper was presented at the 47th AIAA Aerospace Sciences Meeting Including the New Horizons Forum and Aerospace Exposition[17].

II. Estimation of Power Output and Efficiency

A. Navier–Stokes Flow Solver

The unsteady flowfield around the airfoil section was simulated, using the commercially available computational fluid dynamics package Fluent, version 6.3.26, with an unsteady incompressible pressure-based solver. To discretize convection terms, second-order upwind scheme was used; for diffusion-term discretization, second-order central differencing was employed. For single foil calculations, a second-order-accurate backward implicit scheme was used for time discretization. The second-order time accuracy was achieved by considering a moving reference frame (plunging motion) attached to the airfoil, whereas pitching motion is modeled by rotating the airfoil in the plunging reference frame. The plunging motion of the foil was achieved by the introduction of a source term in the governing equations (both stationary and moving mesh zones in Fig. 3), whereas the pitching motion used a sliding mesh (moving mesh zone in Fig. 3). To account for the addition of the source term in the governing equations, the time-varying velocity inlet boundary condition was used, as employed by Kinsey and Dumas [7]. The details of the implementation of this method are also provided in Ashraf [18].

For tandem foil calculations, the motion employed dynamic meshing (mesh deformation and remeshing), due to the lack of a single moving reference frame, which limited time accuracy to first order. In this case, an inertial (fixed) reference frame is considered, and both pitching and plunging motion are applied via motion of the boundary-layer zone attached to each airfoil. The mesh used for tandem foils is shown in Fig. 4. Since remeshing is used for tandem foil cases, the mesh density is maintained at the same level, regardless of the X_{shift} or the airfoil motion, and this mesh density is sufficient enough to capture and maintain the leading foil vortices as they convect. For the case of a plunging airfoil, the comparison of first-order and second-order time accurate simulation was performed in Ashraf [18], and it was found that the prediction from first-order time

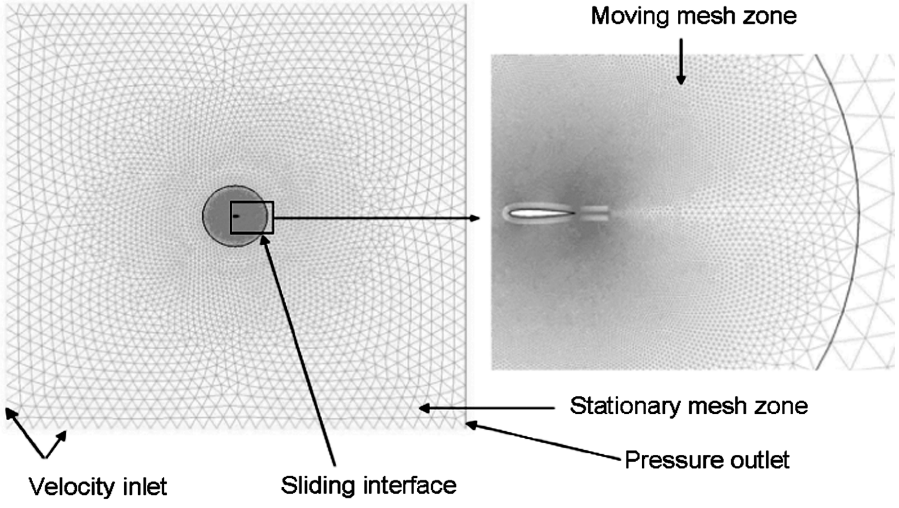

Fig. 3 Details of grid used for single airfoil calculations.

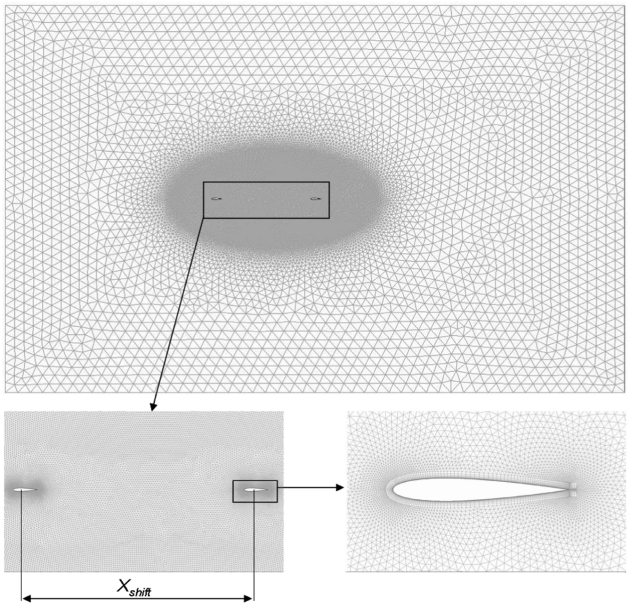

Fig. 4 Details of computational grid used for tandem airfoil calculations.

integration with 800 time steps per cycle is within 3.5% of that of the second-order result, with 800 time steps per cycle.

The mesh used for single and tandem foil calculations is shown in close-up in Fig. 4. The boundary-layer mesh used a first cell distance of 1.0×10^{-5} chord; the pitching element of the mesh was a circle centered on the pitching motion's pivot point, with radius five chords; and the boundaries of the mesh were located at 35 chords upstream of the leading edge and downstream of the trailing edge and at 35 chords from the upper and lower surface of the foil.

The details of grid and time steps per flapping cycle used for grid independence study are given in Table 1. Figure 5 shows the variation of lift for a NACA 0012 airfoil pitching about one-third chord at $Re = 40,000$, $k = 3.39$, $h = 0.25$, and $\theta_o = 25.35°$ under laminar flow conditions. This case has been selected from the force measurement experiments of Anderson et al. [8], for a NACA 0012 airfoil undergoing combined pitching and plunging motion. In this particular case, the kh value (0.85) is comparable to most of the cases considered in this paper ($kh = 0.92$, with $k = 0.88$ and $h = 1.05$). Also, although the frequency is higher than that used for the main part of the study ($k = 0.88$), this is conservative, as the higher frequency leads to smaller LEVs, requiring greater mesh resolution. In Fig. 5, it can be seen that the medium grid, with 800 time steps per flapping cycle, is sufficient to capture the aerodynamic forces on the foil and is used for the remainder of this study.

Table 1 Details of grid and time steps used for grid independence study

Grid	Points on airfoil surface	Time steps per cycle
Coarse (45,740 cells)	100	400, 800, and 3200
Medium (89,078 cells)	200	400, 800, and 3200
Fine (226,562 cells)	400	400, 800, and 3200

As indicated in Sec. I, flapping foils can be used for thrust generation, and there are abundant published data in the literature. The numerical methodology used here is also validated against the experimental results of Heathcote and Gursul [19], and the significance of using a NS solver is highlighted by comparing the results with Garrick's linear analysis [20] in Fig. 6. Heathcote and Gursul [19] performed force measurement experiments on a plunging NACA 0012 airfoil, at a constant plunge amplitude of $h = 0.175$ at different reduced frequencies ($k = 0.0$–12.0). To establish whether turbulence effects would play any significant role at flow $Re = 20,000$, the turbulence model of Spalart–Allmaras [21] is also employed for these validation runs in addition to the laminar case. In Fig. 6, the time-averaged thrust coefficient and propulsive efficiency are plotted against kh. Each case is run for 10 flapping cycles, and the mean is calculated for the last four flapping cycles. The standard deviation in the mean of the last four flapping cycles is plotted as error bars in Fig. 6. It is observed that, for $kh < 1.5$, the NS laminar and turbulent results are identical and are in very good agreement with the experimental data. At this Reynolds-number range and $kh < 1.5$, it is shown by Young and Lai [2] that the increased numerical viscosity introduced by the turbulence model primarily affects the wake behind the plunging airfoil, and the aerodynamic forces are only marginally affected by whether the flow is assumed laminar or turbulent. However, at $kh > 1.5$, there are some minor differences between laminar and turbulent flow simulation results, and both disagree with the experimental data, indicating the presence of transitional flow at higher kh values. Because the maximum kh considered in this paper is $kh < 1.5$, the laminar flow assumption is considered valid and is used for all of the simulations performed in this paper.

For the power extraction regime, we validated our approach against one of the Kinsey and Dumas [7] maximum efficiency cases, at flow $Re = 1100$. As shown in Fig. 7, the coefficient of power plots and $C_{P\text{mean}}$ values agree very well with the results in [7]. In the following sections, the results of numerical simulations for different configurations are discussed in detail.

B. Single Airfoil Sinusoidal Motion

Kinsey and Dumas [7] examined the power extraction performance of a symmetric airfoil (NACA 0015) pitching about one-third chord at $Re = 1100$, for a plunge amplitude $h = 1.0$ with pitching leading plunging by 90° phase. They found a peak efficiency of approximately 34% for pitch amplitudes of 70–80° and reduced frequencies of 0.75–1.1. It must be pointed out that the power coefficient here follows the definition used by Kinsey and Dumas [7], which is referred to the wing area (chord times unit span). However, for conventional wind turbines, the swept area is generally used, giving power coefficients around 0.4 for high-performance turbines. The definition of efficiency here is based on the swept area and can be directly compared with the efficiency of conventional wind turbines, which is arguably accepted to be limited by the Betz efficiency [22]. In the case of a two-dimensional flow over a foil undergoing combined pitching and plunging, the swept area per unit span is calculated based on the maximum excursion of the leading or trailing edge of the

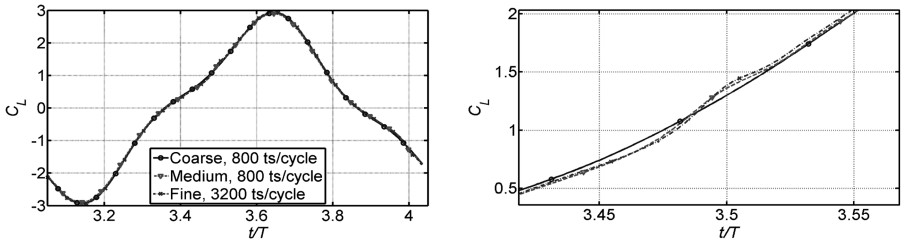

Fig. 5 Instantaneous lift coefficient and zoom view for NACA 0012 airfoil oscillating about one-third chord at $Re = 40,000$, $k = 3.39$, $h = 0.25$, and $\theta_o = 25.35°$.

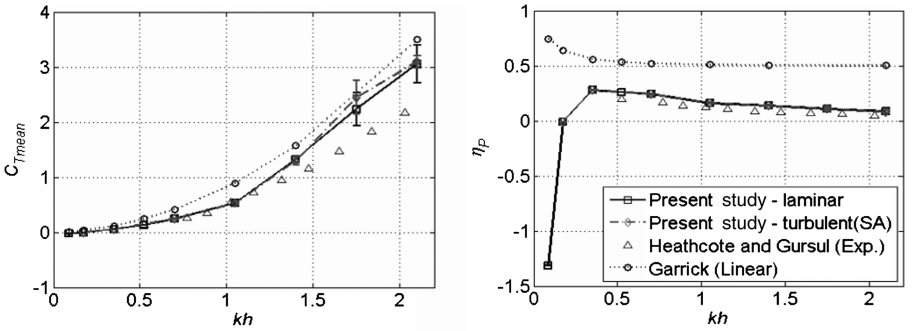

Fig. 6 Variation of $C_{T\text{mean}}$ and η_P with St_{te}, comparison with experimental results of Heathcote and Gursul [19].

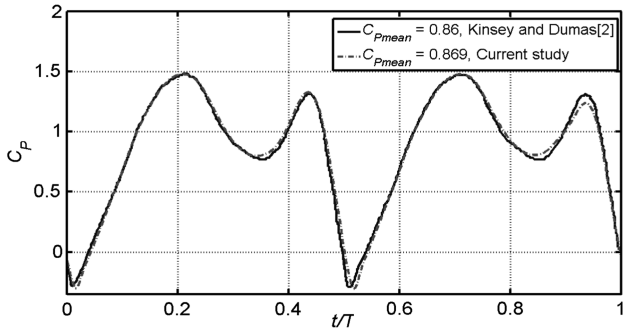

Fig. 7 Instantaneous C_P, comparison with numerical results of Kinsey and Dumas [7] of a NACA 0015 airfoil pitching about one-third chord with $k = 0.88$, $h = 1$, $\theta_o = 76.33°$, and $\phi = 90°$.

foil during the flapping cycle. The swept area per unit span is typically equal to or slightly greater than twice the plunge amplitude.

We examined the effect of varying the phase between pitching and plunging, for a single NACA 0014 airfoil pitching about one-half chord at $Re = 20,000$, $k = 0.8$, $h = 1.05$, and $\theta_o = 73°$. These parameter values have been considered here because they fall in the range for maximum power output and efficiency, as predicted by Kinsey and Dumas [7], and in the range for the experiments conducted by Platzer and his associates [9,10,12]. The NACA 0014 airfoil was chosen for this study because it was used in the tandem hydrofoil power generator [12] described in Sec. I. We found efficiencies consistent with those reported by Kinsey and Dumas [7], as shown in Fig. 8, with a relatively broad power coefficient and efficiency peak over a phase range from 90 to 110°.

For these conditions, the peak power coefficient and maximum efficiency were found at a phase of $\phi = 95°$. In the range $\phi =$ 90–110°, the power coefficient and efficiency are very close to the maximum. Interestingly, this is in very good agreement with the experimental results of McKinney and DeLaurier [1], using a NACA 0012 section wing of aspect ratio 5.25 pitching about one-half chord, $h = 0.3$, $\theta_o = 25$–30°, Reynolds number approximately 85,000–110,000, and $k = 0.39$–0.71. At $Re = 20,000$, the time-averaged results show some variability cycle to cycle, as shown in Fig. 9. Each simulation was run for 15 flapping cycles, and the mean of the last 12 flapping cycles is presented with the standard deviation as error bars, as shown in Fig. 8. One of the cases, $\phi = 90°$, was simulated at $Re = 1100$, and the time-averaged value of power output was compared with the $Re = 20,000$ case. The time history and time-averaged values of two different Reynolds-number simulations are shown in Fig. 9. It shows that at $Re = 20,000$, due to cycle-to-cycle variability, the standard deviation is higher than that of $Re = 1100$, but the mean value remains the same.

Figure 10 shows time histories (phase-averaged over the last 12 flapping cycles) of the translational, rotational, and total power coefficient for $\phi = 70$, 90, 110, and 130°. For 70 and 130°, significant positive power is generated in the upstroke and downstroke, but this is counterbalanced by large negative power during the period of high rotation rate. In contrast, $\phi = 90$ and 110° show only very small negative power peaks during foil rotation, and positive power is maintained for a longer time in the upstroke and downstroke.

To examine the differences in the power extraction between $\phi =$ 70 and 110°, the vorticity contours and surface pressure coefficient distributions at various phases of a flapping cycle are plotted in Fig. 11. It can be seen that, for $\phi = 70°$, significantly large negative power is produced at $t/T = 0.3$ and 0.8 when high lift is generated due to the increased suction caused by the LEVs, and the airfoil is moving in the opposite direction to the lift. On the other hand, for $\phi = 110°$, when the lift generated is in the opposite direction to the motion at $t/T = 0.2$ and 0.7, the lift generated is very small due to the

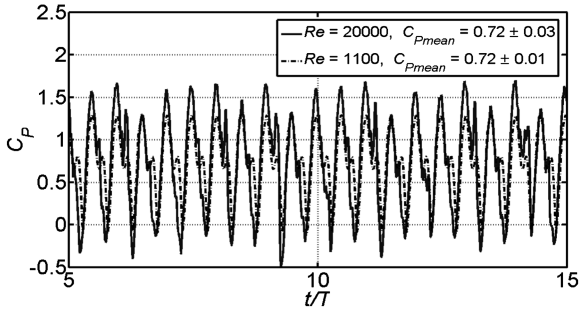

Fig. 9 Instantaneous power coefficient for different Reynolds number, NACA 0014 airfoil pitching about one-half chord at $Re = 20,000$, $k = 0.8$, $h = 1.05$, $\theta_o = 73°$, and $\phi = 90°$.

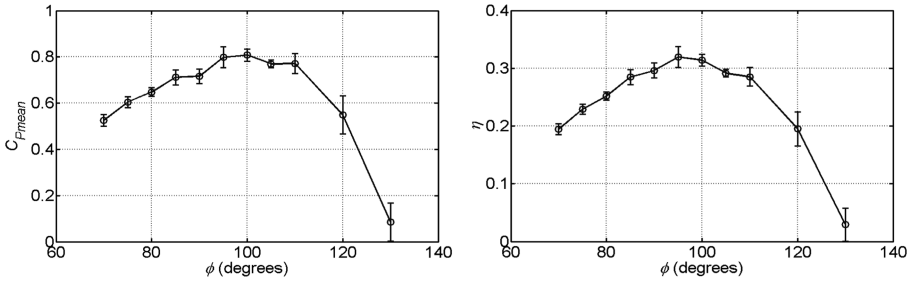

Fig. 8 Time-averaged power coefficient and efficiency vs phase angle between pitch and plunge, NACA 0014 airfoil pitching about one-half chord at $Re = 20,000$, $k = 0.8$, $h = 1.05$, and $\theta_o = 73°$. Error bars indicate standard deviation of time-averaged values.

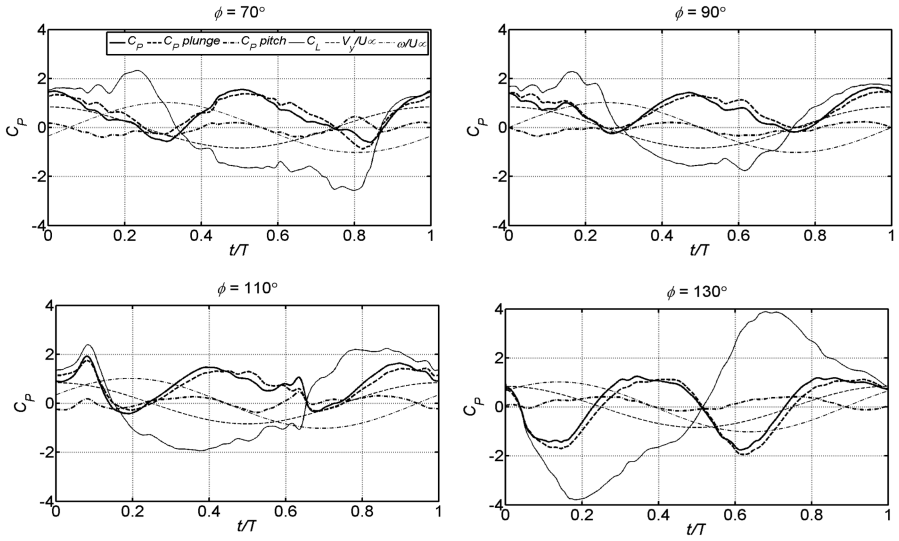

Fig. 10 Instantaneous power coefficient and translational and rotational components for various phases, other flapping parameters as in Fig. 8, airfoil vertical velocity V_y/U_∞ provided as reference.

stall caused by the LEVs, resulting in separation over most of the upper surface, hence, resulting in very small negative power. Overall, $\phi = 110°$ provides better synchronization between lift and motion of the airfoil, which is the case for high power output and high-efficiency cases ($\phi = 90$–$110°$).

For a fixed phase of $\phi = 90°$, Kinsey and Dumas [7] also reported similar results and noted that, for positive power extraction, better synchronization of lift and direction of plunging velocity of airfoil along with the magnitude of lift and plunging velocity of airfoil are very important. They reported that well-timed LEVs are necessary for better synchronization of lift and plunging velocity. They only considered the role of frequency and amplitude of motions to achieve this objective. Here, it is shown that by varying the phase difference between pitching and plunging motions of the airfoil, the timing of LEVs can be adjusted, and better synchronization of lift and plunging velocity could be achieved, which is vital for positive power output.

C. Single Airfoil Nonsinusoidal Motion

Kinsey and Dumas [7] noted that, for the sinusoidal cases studied, where high power coefficients were generated, the contribution to power is significantly dominated by the plunging motion compared with the pitching motion. Their findings, as well as ours, displayed in

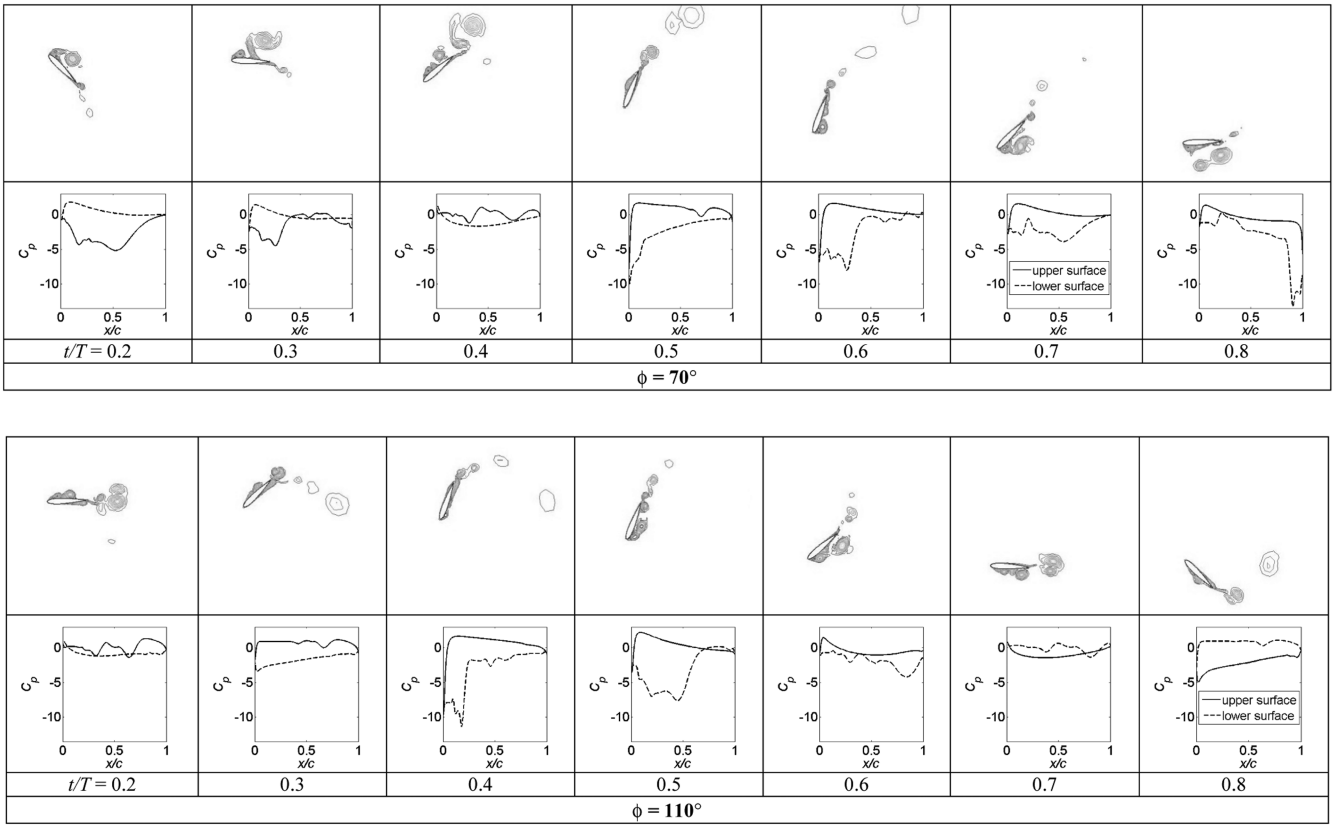

Fig. 11 Vorticity contours and surface pressure coefficient distributions at various points in the flapping cycle for $\phi = 70$ and 110°, other parameters as in Fig. 8.

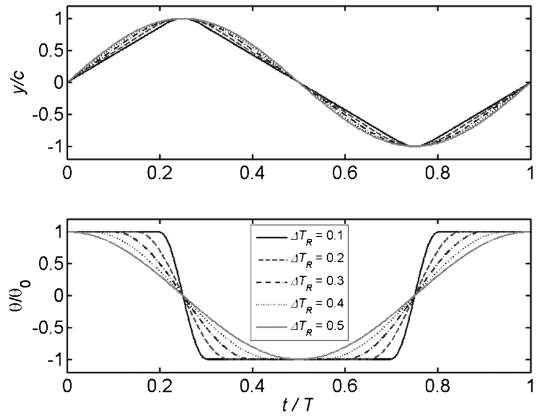

Fig. 12 Variation of plunge and pitch motions simulated.

Figs. 10 and 11, suggest that an alternative airfoil motion may be preferable, in which the airfoil plunge is maintained for as long as possible at a high velocity, followed by rapid pitching reversals. The aerohydrodynamically controlled generator [13,23] oscillates non-sinusoidally in just such a manner as described in Sec. I. The motion of the generator is approximated in Fig. 12, with a period of constant translational velocity combined with a constant pitch angle, followed by a sinusoidal reversal of direction and pitch angle. The equations used to generate the nonsinusoidal motion are given in the Appendix. The pitch motion was smoothed using a Butterworth filter, to avoid a step change in pitch acceleration. The motion is shown with varying reversal times as a fraction of the total cycle ΔT_R, ranging from $\Delta T_R = 0.1$ for rapid reversal to $\Delta T_R = 0.5$ for purely sinusoidal motion. The pitching motion is shown leading the plunge by phase $\phi = 90°$; for other phases, the pitching motion is shifted left or right appropriately.

For comparison of the aerohydrodynamically controlled motion with the usual sinusoidal motion, we selected four phases based on the results in Fig. 10: $\phi = 70$ and 130° where the sinusoidal power and efficiency are low, and $\phi = 90$ and 110° at the locations where the power and efficiency are close to peak values. For these cases, reversal times in the range $\Delta T_R = 0.1$–0.5 are considered. All other flapping parameters are kept the same, namely, $k = 0.8$, $h = 1.05$, and $\theta_o = 73°$. These results are shown in Fig. 13.

For these particular flapping parameters, $\phi = 90°$ appears to be advantageous in terms of both power and efficiency at all the reversal times ΔT_R considered, except at $\Delta T_R = 0.4$ and 0.5 (sinusoidal motion). In fact, the results indicate that $\Delta T_R = 0.3$ and $\phi = 90°$ produce higher power ($C_{P\text{mean}} = 0.89$) and greater efficiency ($\eta = 0.34$) than for any of the sinusoidal motions considered in Fig. 8. Figure 14 shows how the power generation in the non-sinusoidal cases is heavily influenced by the rotation rate of the foil. For small ΔT_R (rapid rotation during stroke reversal), there is a large power input (negative power) required to initiate the foil rotation, followed by a positive power output once the rotation has been established. This rotational power input decreases, and the translational power output during the downstroke and upstroke becomes more uniform, as ΔT_R increases.

To check whether these optimal values of ϕ and ΔT_R are dependent on plunge and pitch amplitudes, similar simulations were run for lower values of plunge and pitch amplitudes $h = 0.5$ and $\theta_o = 40°$. As shown in Fig. 15a, the results for the smaller plunge amplitude $h = 0.5$ show that both $C_{P\text{mean}}$ and η are less sensitive to the phase ϕ, especially for $\Delta T_R > 0.2$. The overall net power

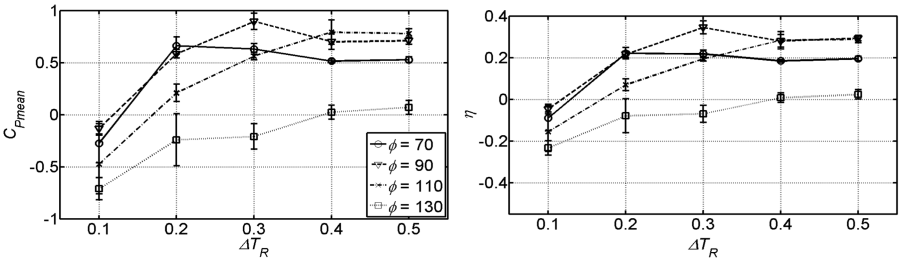

Fig. 13 Time-averaged power coefficient and efficiency for nonsinusoidal motion vs reversal time ΔT_R, $h = 1.05$, and $\theta_o = 73°$, other parameters as in Fig. 8.

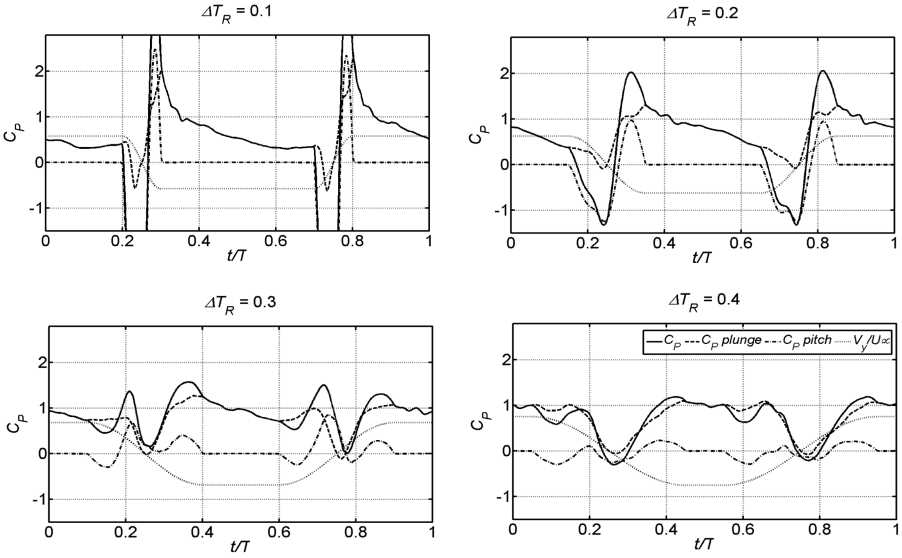

Fig. 14 Instantaneous power coefficient and translational and rotational components for nonsinusoidal motion with various reversal times, $\phi = 90°$, other flapping parameters as in Fig. 8, airfoil vertical velocity V_y/U_∞ provided as reference.

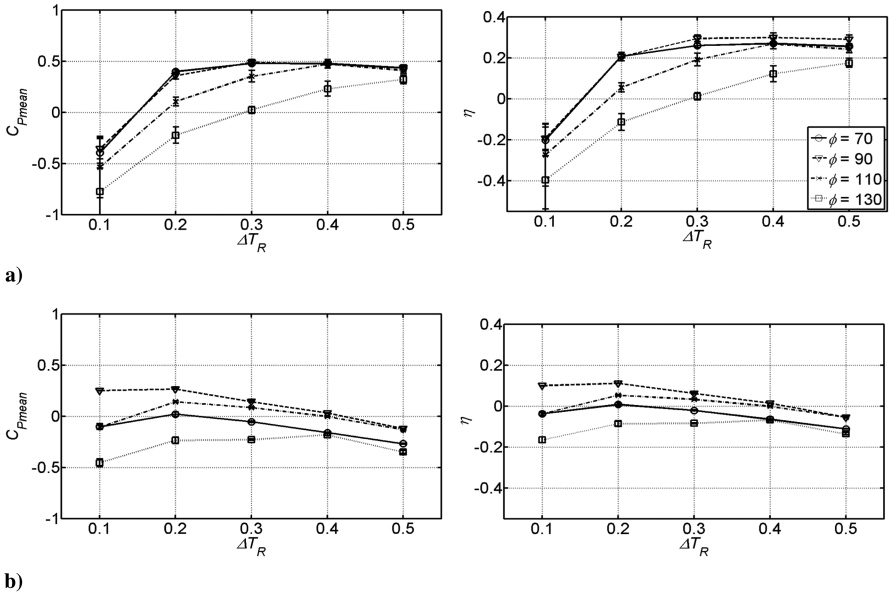

Fig. 15 Time-averaged power coefficient and efficiency for nonsinusoidal motion vs reversal time ΔT_R, $h = 1.05$, and $\theta_o = 73°$, other parameters as in Fig. 8: a) $h = 0.5$ and b) $\theta_o = 40°$.

coefficient and efficiency for $h = 0.5$ are reduced, as expected, due to low peak translational velocity ($V_y = kh$). Further, the results for low values of pitching amplitude $\theta_o = 40°$, in Fig. 15b, show behavior quite different from that for $\theta_o = 73°$. While the net power output for $\theta_o = 40°$ is still influenced by the sharp rotation about the pivot point at the stroke reversal, as shown in Fig. 16, the overall influence is smaller at low values of ΔT_R than for $\theta_o = 73°$, and, once the airfoil is through the rotational power loss, it maintains a more consistent power output during the plunge-only portion of the cycle. For $\theta_o = 40°$, only $\phi = 90°$, $\Delta T_R = 0.1$–0.4 and $\phi = 110°$, $\Delta T_R = 0.2$–0.3 provide positive power outputs, which are still very low compared with the $\theta_o = 73°$ cases. The advantage of high-pitch amplitudes for power generation is also supported by the previous study of Kinsey and Dumas [7].

For a single foil nonsinusoidal power generator, finally, we examined the effect of the reduced frequency on the power generation. We selected the case having maximum $C_{P\text{mean}}$ and η among the tested cases of nonsinusoidal motion with $\Delta T_R = 0.3$, $\phi = 90°$, $h = 1.05$, $\theta_o = 73°$, and airfoil pitching about one-half chord at $Re = 20,000$. The results, in Fig. 17, show a peak in $C_{P\text{mean}}$ (0.89) and η (0.34) for an optimal frequency range $k = 0.7$–1. As also observed by Kinsey and Dumas [7], in their parametric study for a single sinusoidally oscillating power generator, there is a similar optimal frequency range $k = 0.75$–1.13 for peak $C_{P\text{mean}}$ and η at $Re = 1100$. At k values below this range, the plunging velocity ($V_y = kh$) remains very low, resulting in lower $C_{P\text{mean}}$ and η values. At k values above this range, although the plunging velocity is higher, the effective angle of attack reduces, which causes reduction in lift and, therefore, reduction in $C_{P\text{mean}}$ and η. Also, it is important to note that further increase in k or h while keeping everything else constant causes the airfoil to become a propulsion device (at $k = 1.5$, negative power output, as shown in Fig. 17).

Furthermore, Xiao et al. [24] recently presented a NS analysis of flow over a single flapping NACA 0012 airfoil section undergoing nonsinusoidal motion at $St(2kh/\pi) = 0.1$–0.3, $h = 0.5$, $\phi = 90°$, and $Re = 10^4$. They reported that nonsinusoidal motion increases the power output and efficiency of a single airfoil power generator by around 50% over their tested range of parameters. Their findings are

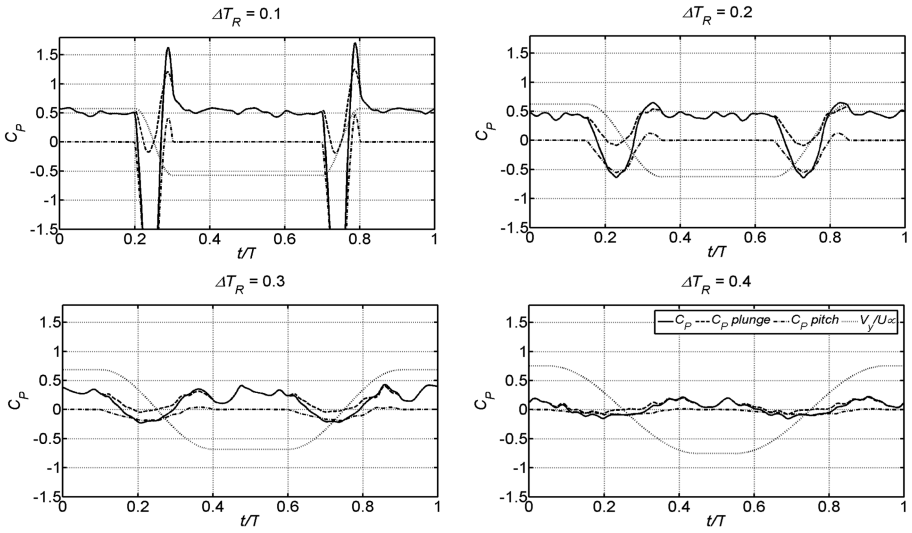

Fig. 16 Instantaneous power coefficient and translational and rotational components for nonsinusoidal motion with various reversal times, $\phi = 90°$ and $\theta_o = 40°$, other flapping parameters as in Fig. 8, airfoil vertical velocity V_y/U_∞ provided as reference.

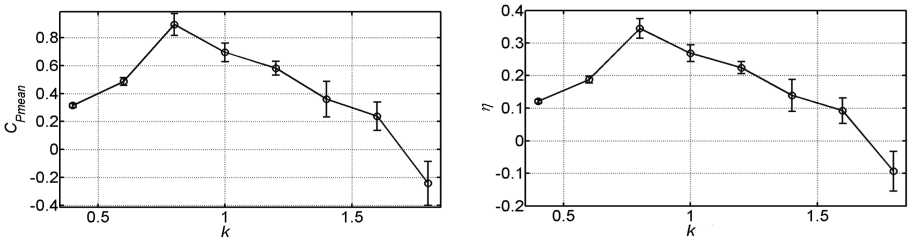

Fig. 17 Time-averaged power coefficient and efficiency for nonsinusoidal motion vs k, other parameters as in Fig. 8.

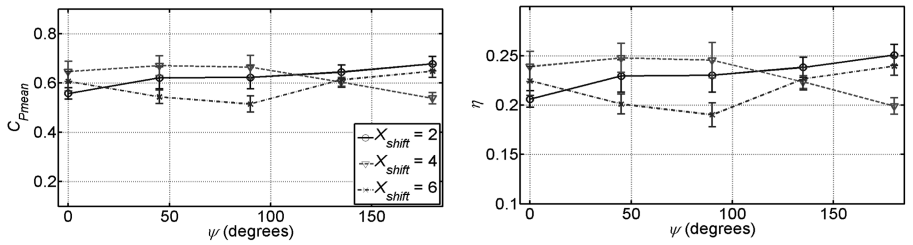

Fig. 18 Total time-averaged power coefficient for tandem foils undergoing sinusoidal motion, individual foil $\phi = 110°$, other flapping parameters as in Fig. 8, effect of distance between foil pivot points X_{shift} and phase ψ between leading and trailing foils assessed.

consistent with our results, which show an increase in power output and efficiency performance of around 17% for an oscillating-wing power generator undergoing nonsinusoidal motion vs sinusoidal motion.

D. Tandem Airfoil Sinusoidal Motion

Here, we examine the power generation obtained from close coupling of two flapping foils in tandem. As for the single foil cases, a NACA 0014 airfoil pitching about one-half chord at $Re = 20,000$, $k = 0.8$, $h = 1.05$, and $\theta_o = 73°$ was used. The motion was sinusoidal, and we selected pitch leading plunge by $\phi = 110°$ for each individual foil. It is important to note here that the performance of two foils operating in close coupling cannot directly be compared with a single foil generator, because if the foils are very close with the same phase of motion, they will effectively act as a single foil with twice the chord length. Keeping the plunge amplitude the same as for a single foil puts them at a disadvantage, because, for optimal power output, one should use the same plunge amplitude as the chord of the foil. On the other hand, if the power output of the tandem foils is referred to the same swept area, then it can lead to efficiencies close to or greater than the Betz efficiency, if the trailing foil is sufficiently far downstream so that the velocity deficiency generated by the leading foil has been filled by the outer flow. In other words, additional foils

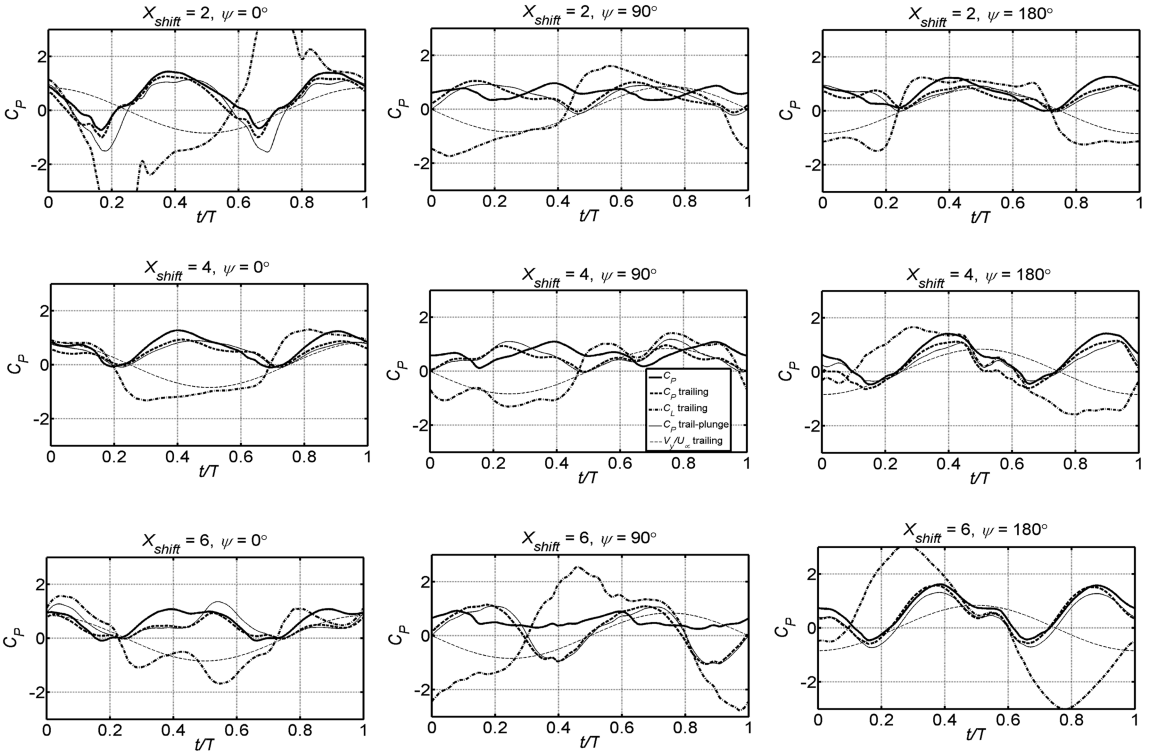

Fig. 19 Total instantaneous power coefficient and contributions from leading and trailing foils for tandem foils undergoing sinusoidal motion (details in Fig. 18), leading and trailing foil vertical velocity V_y/U_∞ provided as reference.

can be put into the same swept area of the first foil, and power can be extracted. An interesting question would then be if the same amount of power can be extracted by the leading foil if the trailing (and additional) foils are located sufficiently far downstream. This answer can probably best be obtained by using potential flow theory (i.e., by using a panel method analysis) but not by using actuator disk theory. This would give the upper limit (similar to the Betz theory). On the other hand, moving the trailing foil close to the leading foil should approach the performance of a single foil with the same total chord length. This performance must be significantly below the Betz limit, because actuator theory involves only foils with "zero" chord length. Further, it is also obvious that the velocity deficiency caused by the leading foil reduces the available power for the trailing foil, and, therefore, in current NS analysis, the combined power output (sum of $C_{P\text{mean}}$ of leading and trailing foils) cannot exceed twice the $C_{P\text{mean}}$ of a single foil. With the tandem foil generator, one can only approach the limit of twice the $C_{P\text{mean}}$ of single foil if the foils are placed sufficiently far apart and the phase of motion of foils is such that velocity deficiency of leading foil and wake interaction do not influence the trailing foil. In that case, the loss and capital cost associated with connecting mechanism would offset the gain acquired.

To assess the performance of the tandem foil generator, we use the averaged power coefficient and the efficiency per foil in tandem configuration. The effect of the phase ψ between the leading and trailing foils and the distance between the two pivot points X_{shift} is assessed, with the results given in Figs. 18–20. Figure 18 shows that the power and efficiency results are sensitive to both ψ and X_{shift}, indicating that the system may need to be tuned (via varying ψ and X_{shift}) to achieve optimal placement of the trailing foil in the vortex wake of the leading foil, as the flow speed varies. Also, examination of the time histories in Fig. 19 shows that, although for cases with $X_{\text{shift}} = 2$, 4, and 6 and $\psi = 0°$, as well as for the case with $X_{\text{shift}} = 4$ and $\psi = 180°$, positive net power is generated, there are periods when the foils are at the end of upstroke or downstroke ($t/T = 0.25$ and 0.75) in which the total power contribution of the two foils drops below zero, and, hence, the system would not be self-driving (for clarity, $\psi = 45$ and 135° time histories are not shown here).

At $X_{\text{shift}} = 2$ and $\psi = 0°$, during the stroke reversal, high lift is generated from the trailing foil because of the interaction with the vortex wake of the leading foil, but the translational velocity of the trailing foil has opposite sign to the lift, as seen in Fig. 19, at $t/T = 0.2$ and 0.7. In comparison, at $X_{\text{shift}} = 2$ and $\psi = 180°$, although less lift is generated, the phase difference between the foils provides better synchronization of lift with the translational velocity, resulting in net positive power output being maintained throughout the whole cycle.

By increasing the X_{shift}, at $\psi = 0°$, the influence of the leading foil wake becomes weaker, and less lift force is generated, compared with the $X_{\text{shift}} = 2$ case. The poor synchronization of lift with the trailing foil's translational velocity still causes the net power to drop down to below zero, as shown in Fig. 21. For $\psi = 45$ and 90°, placing the trailing airfoil farther away in the wake again causes the negative interaction with the wake and the lesser lift (in the cases of $X_{\text{shift}} = 4$ and 6 and $\psi = 45°$ and $X_{\text{shift}} = 4$ and $\psi = 90°$), and the poor synchronization of the lift and translational velocity (in the case of $X_{\text{shift}} = 6$ and $\psi = 90°$) causes overall power generation to fall, as the plots show in Fig. 19.

The details of the negative interaction between the vortex wake of the leading foil with the trailing foil due to the influence of X_{shift} and ψ are illustrated in the vorticity contour plots in Fig. 20. For a given $X_{\text{shift}} = 2$, the influence of ψ at $t/T = 0.2$ and 0.25 can be seen in Figs. 20a and 20b, for $\psi = 0°$ and 180°, respectively. For $\psi = 0°$, at these instants, the wake of the leading foil strikes the leading edge of the trailing foil and creates large amount of lift when the trailing foil moves in the opposite direction to lift. For $\psi = 180°$, the same vortices have been avoided by the trailing foil, resulting in less amount of lift and, thus, less reduction in net power.

For a given $\psi = 90°$, the influence of X_{shift} at $t/T = 0.4$ and 0.45 can be seen in Figs. 20c and 20d, for $X_{\text{shift}} = 2$ and 6, respectively. At $X_{\text{shift}} = 2$, the lift of the trailing foil is synchronized with the velocity of the trailing foil (see Fig. 19), because the wake of the trailing foil avoids the interaction with the main vortex shedding off the leading foil, due to a better placement of the foil in the wake. On the other hand, at $X_{\text{shift}} = 6$, the vortex wake of the leading foil interacts negatively on the upper surface of the trailing airfoil, causing a large lift opposite to that of the velocity of the trailing foil at $t/T = 0.4$ and 0.45 (see Figs. 20c and 20d). This supports the argument that the system of two foils must be tuned for best power output based on the placement of the trailing foil. We note, in Fig. 18, that, for the current

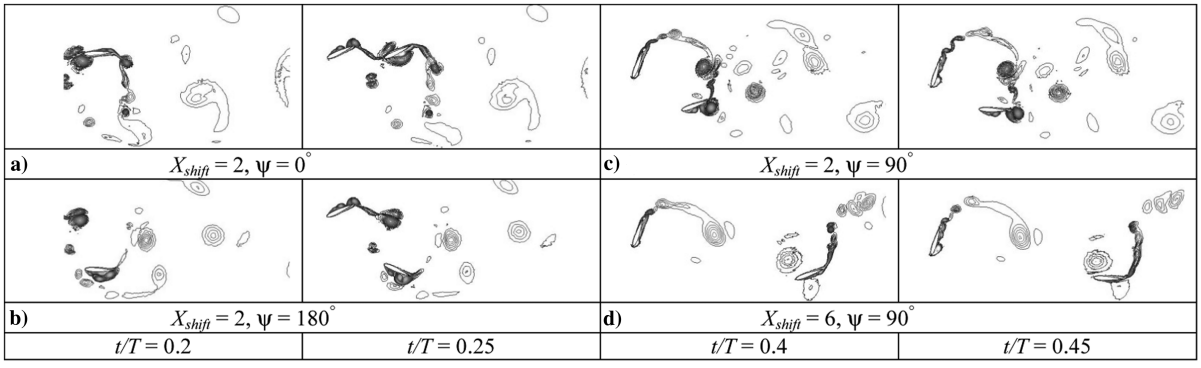

Fig. 20 Vorticity contours for tandem foils undergoing sinusoidal motion at different instants during flapping cycle.

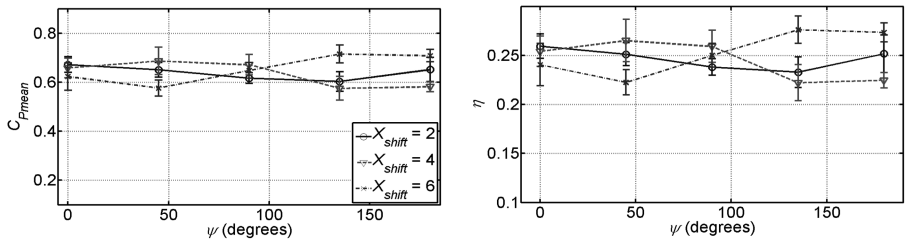

Fig. 21 Total time-averaged power coefficient for tandem foils undergoing nonsinusoidal motion, individual foil $\Delta T_R = 0.3$, other flapping parameters as in Fig. 8, effect of distance between foil pivot points X_{shift} and phase ψ between leading and trailing foils assessed.

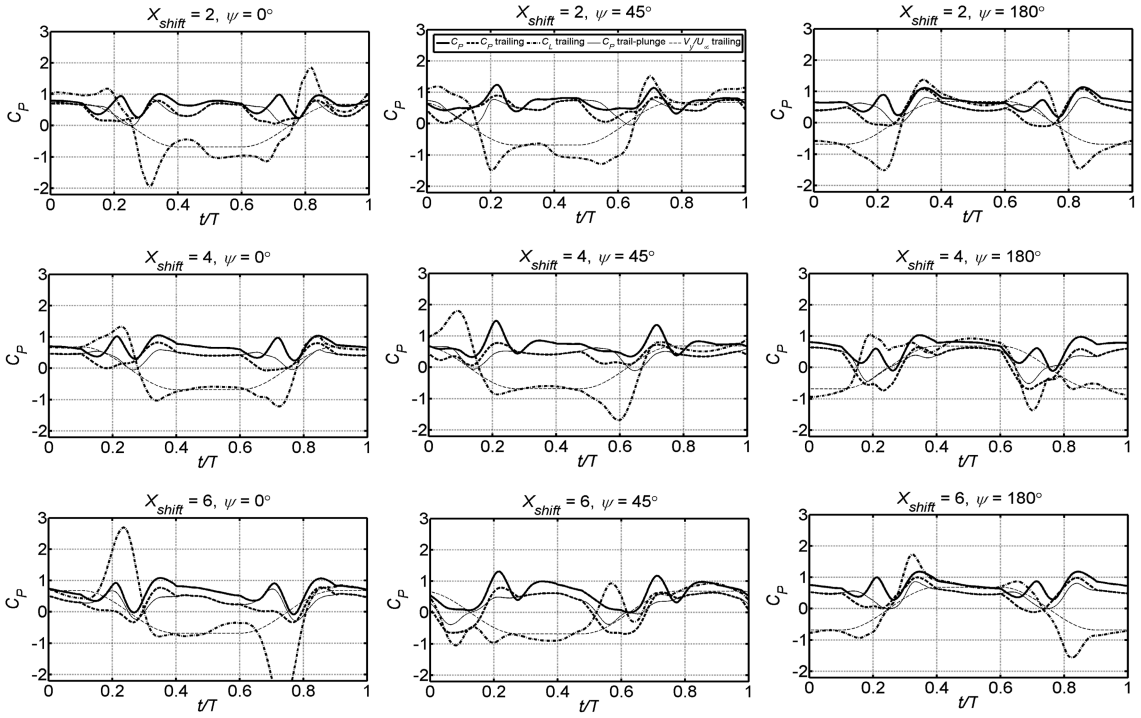

Fig. 22 Total instantaneous power coefficient and contributions from leading and trailing foils for tandem foils undergoing nonsinusoidal motion (details in Fig. 21), leading and trailing foil vertical velocity V_y/U_∞ provided as reference.

study, $X_{\text{shift}} = 4$ and $\psi = 0$ to 90° and $X_{\text{shift}} = 2$ and $\psi = 135$ and 180° appear to be the better choice for a sinusoidal tandem power generation system.

E. Tandem Airfoil Nonsinusoidal Motion

Based on the results discussed in Sec. II.C, we now examine the power generation from close coupling of two flapping foils undergoing nonsinusoidal motion. As for the single foil nonsinusoidal cases, a NACA 0014 airfoil pitching about one-half chord, $k = 0.8$, $h = 1.05$, and $\theta_o = 73°$ was used. We selected the stroke reversal time, $\Delta T_R = 0.3$ and $\phi = 90°$, for each individual foil, based on the single foil results of Fig. 13. The effect of varying the phase ψ between leading and trailing foils and the distance between the two pivot points X_{shift} is evaluated, as shown in Figs. 21–23. Similar to the sinusoidal tandem power generation, Fig. 21 shows that, for nonsinusoidal motion, the results are sensitive to both ψ and X_{shift}, again indicating that the trailing foil needs not only to be placed optimally in the vortex wake of the leading foil but also the phase of trailing foil motion to be adjusted optimally. All the values of ψ and X_{shift} tested appear to generate net positive power, as shown in Fig. 21. However, further examination of phase-averaged time histories in Fig. 22 reveals that, for $X_{\text{shift}} = 6$ and $\psi = 0°$ and $X_{\text{shift}} = 4$ and $\psi = 180°$, for a small duration near the end of the upstroke (at $t/T = 0.25$) and the end of the downstroke (at $t/T = 0.75$), the total power contribution of the two foils is negative, and, therefore, the system would not be self-driving (for clarity, $\psi = 90$ and 135° time histories are not shown here).

Figure 23 shows how the interaction between the wake of the leading foil and the trailing foil affects the overall power coefficient. For $X_{\text{shift}} = 4$ and $\psi = 45°$, at $t/T = 0.5$–0.6 the main vortex in the wake of the leading foil helps create the suction on the lower surface

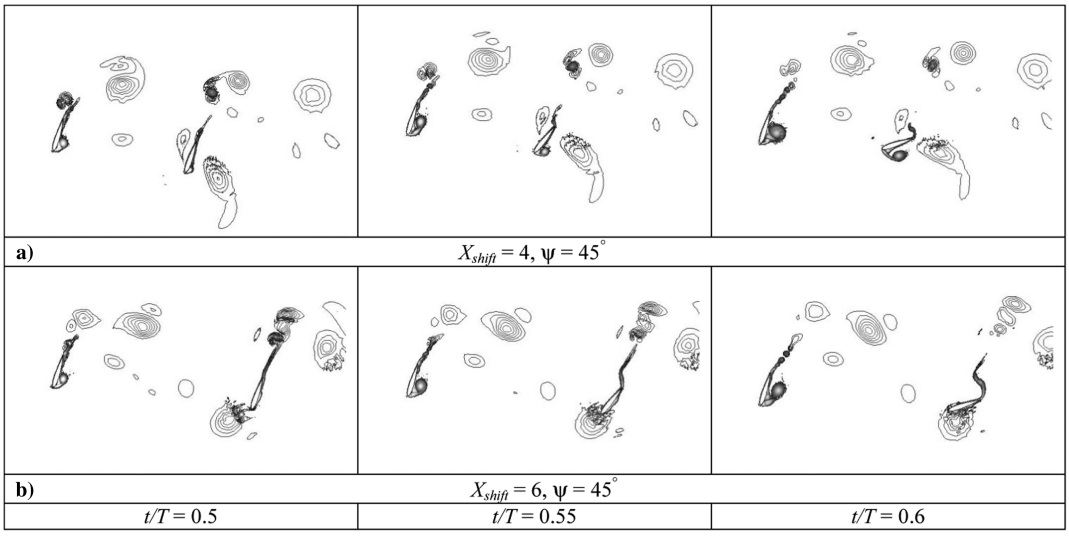

Fig. 23 Vorticity contours for tandem foils undergoing nonsinusoidal motion at different instants during flapping cycle.

Table 2 Maximum $C_{P\text{mean}}$ and η for different configurations of airfoils flapping at $k = 0.8$, $h = 1.05$, and $\theta_o = 73°$ at $Re = 20,000$

Configuration	$C_{P\text{mean}}$ leading foil	$C_{P\text{mean}}$ trailing foil	$C_{P\text{mean}}$ per foil	η per foil
Single foil sinusoidal ($\phi = 95°$)	——	——	0.84 ± 0.04	0.32 ± 0.02
Single foil nonsinusoidal ($\Delta T_R = 0.3$ and $\phi = 90°$)	——	——	0.89 ± 0.07	0.34 ± 0.03
Sinusoidal tandem ($\phi = 110°$, $X_{\text{shift}} = 2$, and $\psi = 180°$)	0.80 ± 0.05	0.56 ± 0.01	0.68 ± 0.03	0.25 ± 0.02
Nonsinusoidal tandem ($\Delta T_R = 0.3$, $\phi = 90°$, $X_{\text{shift}} = 6$, and $\psi = 135°$)	1.00 ± 0.04	0.43 ± 0.05	0.72 ± 0.04	0.27 ± 0.05

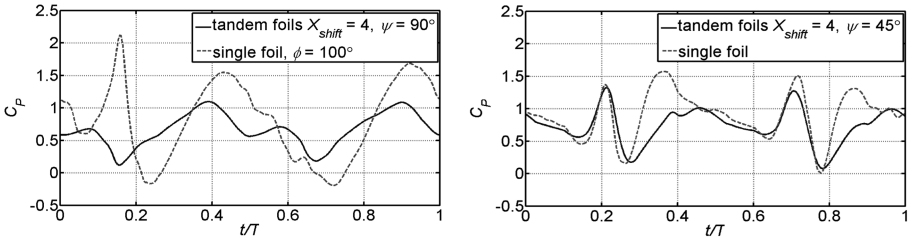

a) b)

Fig. 24 Comparison of total instantaneous power coefficient of single and tandem foil power generators undergoing a) sinusoidal motion and b) nonsinusoidal motion.

of the trailing foil, which generates high lift in the same direction as the translational velocity of the trailing foil (see vorticity contour plots in Fig. 23a at $t/T = 0.5$–0.6), and, hence, positive power is produced. On the other hand, for $X_{\text{shift}} = 6$ and $\psi = 45°$, the same vortex from the leading foil strikes the leading edge of the trailing foil, due to increased X_{shift}, resulting in a lift of opposite sign to the translational velocity, and, hence, negative power is produced at $t/T = 0.5$–0.6 (see Fig. 23b), reducing the overall power output. In the range of values tested, $X_{\text{shift}} = 4$ and $\psi = 45°$ and $X_{\text{shift}} = 6$ and $\psi = 135$ and 180° appear to be the best choice of parameters, based on the $C_{P\text{mean}}$ values as shown in Fig. 21.

F. Comparison of Different Configurations

Here, we present an overall comparison of power extraction performance for all the configurations examined in the present study. Table 2 shows the maximum $C_{P\text{mean}}$ output and η for the best of each configuration assessed. It is evident that, for a single foil generator, the nonsinusoidally driven foil generates more power (17%) more efficiently (15%) than the sinusoidally driven generator. Further, using two foils in tandem, either sinusoidally driven or nonsinusoidally driven, appears to be more attractive in terms of smoothing out the power time history and also generating positive power throughout the flapping cycle, making the system self-driving for most of the cases examined. Also, if there is any limitation on the plunge amplitude due to space restriction in shallow water streams, the use of two or more foils in tandem would be practical to enhance the power output. A comparison of the time history of the combined power output of a tandem foil generator with a single foil generator undergoing sinusoidal motion (maximum power output case; see Sec. II.B) is shown in Fig. 24a. Similar comparison for generators undergoing nonsinusoidal motion is displayed in Fig. 24b. It is clear from Fig. 24 that, although the averaged power output capacity per foil of the tandem foil generator is lower than that of a single foil generator, the power output curve of the tandem foil generator remains positive throughout the flapping cycle, indicating the self-driving capability of the tandem foil generator. On the other hand, the single foil generator outperforms the tandem foil generator in efficiency by over 20%. It is also important to be reminded that, for both power output and efficiency, this study does not take into account the mechanical losses associated with mechanism linking the two foils. Therefore, a direct comparison of the performance of power generation cannot be made between the single and tandem configurations. Nevertheless, comparison of the two tandem configurations reveals that nonsinusoidal motion is again more efficient (6% more) than the sinusoidal counterpart.

III. Conclusions

The power extraction potential of flapping airfoils in different configurations has been explored using NS two-dimensional laminar flow calculations for a NACA 0014 foil at $Re = 20,000$. The study of the effect of phase difference between pitching and plunging motion on the power extraction through a sinusoidally flapping foil showed that power output and efficiency peak in the range of $\phi = 90$–$110°$. By using an aerohydrodynamically inspired nonsinusoidal motion, power extraction efficiency as high as 34% and $C_{P\text{mean}} = 0.89$ can be achieved for a single foil oscillating at $k = 0.8$, $h = 1.05$, $\theta_o = 73°$, $\Delta T_R = 0.3$, and $\phi = 90°$. In this case, the plunging component of power output dominates the overall power output from the oscillating airfoil. Further, both sinusoidal and nonsinusoidal motions for potential power generators with two foils flapping in tandem were explored. It was found that the trailing foil could be placed at an optimal distance X_{shift} with an optimal phase difference to extract maximum power output for the generator at given amplitudes of motion and Reynolds number. An $X_{\text{shift}} = 4$ chords distance between leading and trailing foil pivot points was found to generate higher power at a higher efficiency (around 7% more) than either $X_{\text{shift}} = 2$ or 6, when the phase difference between the motion of the two foils is less than 90° for both sinusoidal and nonsinusoidal tandem cases. For phase difference 135 and 180° sinusoidal tandem cases, $X_{\text{shift}} = 2$ generates higher power at higher efficiency (around 5%) than $X_{\text{shift}} = 4$ and 6. For phase difference 135 and 180° nonsinusoidal tandem cases, $X_{\text{shift}} = 6$ generates higher power at higher efficiency than $X_{\text{shift}} = 2$ and 4. These results may be dependent on the Reynolds number, reduced frequency, and motion amplitude. Overall, the results for a single NACA 0014 wing power generator undergoing nonsinusoidal pitch–plunge motion indicates around 17% increase in power generated and around 15% increase in efficiency over that for sinusoidal motion. For sinusoidal motion, in the tandem configuration, both averaged power output and efficiency per foil are reduced by around 20%, compared with a single foil in sinusoidal motion; however, a smoothed-out and positive time history of power output throughout the flapping cycle (i.e., self-starting and self-driving) are advantages of the tandem configuration. For nonsinusoidal motion, a similar reduction in performance is observed for the tandem generator, compared with a single foil generator.

Appendix

Table A1 Equations for generating nonsinusoidal motion

Description	Equations
Start of flapping cycle, plunge motion at maximum positive pitch amplitude $t < t_a$[a]	$y(t) = t\dot{y}_{\max}$, where $\dot{y}_{\max} = \frac{2y_{\max}}{T(2\Delta T_R/(\pi+0.5-\Delta T_R))}$; $\theta(t) = \theta_{\max}$
Rotation from maximum positive to negative pitch amplitude $t < t_b$[b]	$y(t) = y_{\lim} + y_{\text{sm}} \sin(\pi/\Delta T_R T(t - t_a))$, where $y_{\lim} = t_a y_{\max}$ and $y_{\text{sm}} = y_{\max} - y_{\lim}$; $\theta(t) = \theta_{\max} \cos(\pi/\Delta T_R T(t - t_a))$
Plunge motion at maximum negative pitch amplitude $t < t_c$[c]	$y(t) = -\dot{y}_{\max}(t - 0.5T)$; $\theta(t) = -\theta_{\max}$
Rotation from maximum negative to positive pitch amplitude $t < t_d$[d]	$y(t) = y_{\lim} - y_{\text{sm}} \sin(\pi/\Delta T_R T(t - t_c))$, where $y_{\lim} = -y_{\max}(t_c - 0.5T)$ and $y_{\text{sm}} = y_{\max} + y_{\lim}$; $\theta(t) = -\theta_{\max} \cos(\pi/\Delta T_R T(t - t_c))$
Plunge motion at maximum positive pitch amplitude, end of flapping cycle $t < t_e$[e]	$y(t) = -\dot{y}_{\max}(t - T)$; $\theta(t) = \theta_{\max}$

[a] t = time; $t_a = (0.25 - 0.5\Delta T_R)T$, where ΔT_R = stroke reversal time as a fraction of the flapping period, and T = period of oscillation.
[b] $t_b = (0.25 + 0.5\Delta T_R)T$.
[c] $t_c = (0.75 - 0.5\Delta T_R)T$.
[d] $t_d = (0.75 + 0.5\Delta T_R)T$.
[e] $t_e = T$.

Acknowledgments

Max F. Platzer acknowledges support of a University of New South Wales at the Australian Defense Force Academy Rector Visiting Fellowship, which initiated some of the computational work reported here. Navier–Stokes calculations by M. A. Ashraf were performed with the support of a grant, under the Merit Allocation Scheme of the National Computational Infrastructure National Facility.

References

[1] McKinney, W., and DeLaurier, J., "The Wingmill: An Oscillating-Wing Windmill," *Journal of Energy*, Vol. 5, No. 2, 1981, pp. 109–115. doi:10.2514/3.62510

[2] Young, J., and Lai, J., "Oscillation Frequency and Amplitude Effects on the Wake of Plunging Airfoil," *AIAA Journal*, Vol. 42, No. 10, 2004, pp. 2042–2052. doi:10.2514/1.5070

[3] Rozhdestvensky, K., and Ryzhov, V., "Aerohydrodynamics of Flapping-Wing Propulsors," *Progress in Aerospace Sciences*, Vol. 39, No. 8, 2003, pp. 585–633. doi:10.1016/S0376-0421(03)00077-0

[4] Young, J., and Lai, J., "Mechanisms Influencing the Efficiency of Oscillating Airfoil Propulsion," *AIAA Journal*, Vol. 45, No. 7, July 2007, pp. 1695–1702. doi:10.2514/1.27628

[5] Shyy, W., Lian, Y., Tang, J., Viieru, D., and Liu, H., *Aerodynamics of Low Reynolds Number Flyers*, Cambridge Univ. Press, Cambridge, England, U.K., 2008, pp. 1–96.

[6] Platzer, M., Jones, K., Young, J., and Lai, J., "Flapping-Wing Aerodynamics: Progress and Challenges," *AIAA Journal*, Vol. 46, No. 9, 2008, pp. 2136–2149. doi:10.2514/1.29263

[7] Kinsey, T., and Dumas, G., "Parametric Study of an Oscillating Airfoil in a Power-Extraction Regime," *AIAA Journal*, Vol. 46, No. 6, 2008, pp. 1318–1330. doi:10.2514/1.26253

[8] Anderson, J., Streitlien, K., Barrett, D., and Triantafyllou, M., "Oscillating Foils of High Propulsive Efficiency," *Journal of Fluid Mechanics*, Vol. 360, 1998, pp. 41–72. doi:10.1017/S0022112097008392

[9] Davids, S., "A Computational and Experimental Investigation of a Flutter Generator," M.S.A.E. Thesis, Naval Postgraduate School, Monterey, CA, 1999.

[10] Lindsey, K., "A Feasibility Study of Oscillating-Wing Power Generators," M.S.A.E. Thesis, Naval Postgraduate School, Monterey, CA, 2002.

[11] Jones, K., Davids, S., and Platzer, M., "Oscillating-Wing Power Generation," *Third ASME/JSME Joint Fluids Engineering Conference*, 1999.

[12] Jones, K., Lindsey, K., and Platzer, M., "An Investigation of the Fluid–Structure Interaction in an Oscillating-Wing Micro-Hydropower Generator," *Fluid Structure Interaction 2*, Southampton, England, U.K., 2003, pp. 73–82.

[13] Platzer, M., Ashraf, M., Young, J., and Lai, J., "Extracting Power in Jet Streams: Pushing the Performance of Flapping Wing Technology," 27th Congress of the International Council of the Aeronautical Sciences, International Council of the Aeronautical Sciences Paper 2010-2.9.1, Nice, France, 19–24 Sept. 2010.

[14] Kaya, M., and Tuncer, I., "Nonsinusoidal Path Optimization of a Flapping Airfoil," *AIAA Journal*, Vol. 45, No. 8, 2007, pp. 2075–2082. doi:10.2514/1.29478

[15] Akhtar, I., Mittal, R., Lauder, G., and Drucker, E., "Hydrodynamics of a Biologically Inspired Tandem Flapping Foil Configuration," *Theoretical and Computational Fluid Dynamics*, Vol. 21, No. 3, 2007, pp. 155–170. doi:10.1007/s00162-007-0045-2

[16] Lehmann, F.-O., "Wing–Wake Interaction Reduces Power Consumption in Insect Tandem Wings," *Experiments in Fluids*, Vol. 46, No. 5, 2008, pp. 765–775. doi:10.1007/s00348-008-0595-0

[17] Platzer, M., Ashraf, M., Young, J., and Lai, J., "Development of a New Oscillating-Wing Wind and Hydropower Generator," 47th AIAA Aerospace Sciences Meeting Including the New Horizons Forum and Aerospace Exposition, AIAA Paper 2009-1211, Orlando, FL, 5–8 Jan. 2009.

[18] Ashraf, M., "Numerical Simulation of the Flow over Flapping Airfoils in Propulsion and Power Extraction Regimes," Ph.D., Dissertation, Univ. of New South Wales at the Australian Defense Force Academy, Canberra, Australia, 2010.

[19] Heathcote, S., and Gursul, I., "Flexible Flapping Airfoil Propulsion at Low Reynolds Number," *AIAA Journal*, Vol. 45, No. 5, 2007, pp. 1066–1078. doi:10.2514/1.25431

[20] Garrick, I., "Propulsion of a Flapping and Oscillating Airfoil," NACA Rept. 567, 1937.

[21] Spalart, P., and Allmaras, S., "A One-Equation Turbulence Model for Aerodynamic Flows," AIAA Paper 1992-0439, 1992.

[22] Lam, G., "Wind Energy Conversion Efficiency Limit," *Wind Engineering*, Vol. 30, No. 5, 2006, pp. 431–437. doi:10.1260/030952406779502687

[23] Platzer, M., Young, J., and Lai, J., "Flapping-Wing Technology: Its Potential for Air Vehicle Propulsion and Airborne Power Generation," 26th Congress of the International Council of the Aeronautical Sciences, International Council of the Aeronautical Sciences Paper 2008-1.5.2, Anchorage, AK, 14–19 Sept. 2008.

[24] Xiao, Q., Liao, W., and Yang, S., "How Motion Trajectory Affects the Energy Extraction Performance of an Oscillating Foil," *48th AIAA Aerospace Sciences Meeting Including the New Horizons Forum and Aerospace Exposition*, Orlando, FL, 2010.

P. Beran
Associate Editor